Particulate phase evolution inside solid rocket motors: preliminary results

S. Carlotti[*][†]*, J. Anfossi*[*]*, R. Bellini*[*]*, G. Colombo*[*] *and F. Maggi*[*]
Politecnico di Milano, Aerospace Science and Technology Dept.
Space Propulsiona Laboratory (SPLab)
via la Masa 34, 20156, Milan, Italy
stefania.carlotti@polimi.it · jody.anfossi@mail.polimi.it · raffaele1.bellini@mail.polimi.it
giovanni.colombo@polimi.it · filippo.maggi@polimi.it
[†]Corresponding author

Abstract

The present work focuses on the alumina particles size evolution inside the nozzle. For this purpose, an experimental and numerical investigation is proposed, focusing on two main topics: (1) development of a novel experimental device enabling nozzle-flow visualization. This apparatus consists of a two-dimensional windowed rocket motor operating at pressure up to 15 bar, recording the propellant burning and flowfield evolution by means of a high speed camera. (2) Coupling of an Eulerian gas phase description and Lagrangian particle tracking in the open-source environment OpenFOAM to simulate clouds of particles of different size in a supersonic environment.

1. Introduction

Many different physical phenomena are involved in the two-phase and reacting flowfield of solid rocket motors (SRMs). Challenges in terms of performance estimation, pollution, thermal and chemical loading arise from the complex physical phenomena governing those systems. Commonly, aluminum powder is used to improve performance, leading at the same time to disadvantages such as formation of condensed combustion products (CCPs), particle accumulation, nozzle erosion, and pollution (i.e., increased primary smoke by exhaust of alumina and contribution to ozone depletion). In the past decades, great effort was put into the definition of the size and composition of the particulate phase, collecting the CCPs in the vicinity of the surface, thus defining the initial condition of alumina particles size distribution (PSD). However, collisions between droplets and breakup events inside the convergent-divergent nozzle greatly cause the modification of the PSD. Hence, it is almost clear that the prediction of the two-phase flow within the combustion and nozzle expansion process must therefore take into account and propose new concepts upon the complex pathways of both the gaseous mixtures and the particulate phase. In particular, the large uncertainties in the state, size, and distribution of alumina need to be deeply investigated and their direct influence on the main flow properly characterized.

Within the current study we focus on the development of two tools for the study of the particulate phase evolution in SRMs. One one hand, an experimental device enabling the visualization of the particles evolution in a gas dynamic nozzle in presence of cross-flow in combustion chamber is proposed. A numerical solver in the open-source environment OpenFOAM, able to describe the multiphase flow in SRMs, is pursued in parallel. In particular, a compressible Eulerian gas phase description is coupled to a Lagrangian particle tracking. The present paper aims at giving an overview and a comparison of the preliminary results of both the methods, highlighting the possibilities these two tools can offer.

2. Experimental Activity

2.1 State of the Art

After the release of aluminum agglomerates from the burning surface, they are still rich of metal and further oxidizer in the core of the rocket, till they reach the nozzle. The product of this oxidation is alumina (Al2O3) which generates a

PARTICULATE PHASE EVOLUTION INSIDE SOLID ROCKET MOTORS: PRELIMINARY RESULTS

two-phase flow of gas-liquid kind. Inside the nozzle, metal drops undergo further modifications. Particles are trailed by the accelerating flow, featuring a velocity and thermal lag. The gaseous fraction decreases its temperature and increases its velocity, while the condensed fraction moves and releases heat slower, creating a surplus in temperature and a deficit in velocity with respect to the other. This effects are related to type, size and shape of the condensed fraction[6] . If the behaviour of a single droplet is considered, particles find the conditions for breakup both in the nozzle convergent and divergent section[9] . However, a cloud of particles must be considered since the SRMs flow can be categorized as extremely dense. Turbulent mixing and differential velocity between particles of different size (e.g., usually the particulate resulting from aluminized propellants shows a bimodal size distribution) generate the conditions for growth due to collision[18] - in particular in the convergent part of the nozzle. In fact, although the larger particles are quickly broken down by the lag-induced shear forces in the nozzle, there is still a large difference in size among the particles and, therefore, velocity; this causes a high-collision frequency at high-impact energies[29] , with possible coalescence.

Several authors have obtained high resolution photographs of aluminized propellants burning as strands in quiescent atmospheres and have photographed the burning surface and agglomerates formed by those burning strand, gaining an overview of the initial conditions of metal particles lifetime. Shadowgraph,[7] holography[1] and high-speed camera[13,21] are the most important techniques employed in this framework. Many details of the metal burning processes are appreciable and different conditions can be investigated to gain an insight on the behaviour of the particles isolated from the shearing forces of the real high-speed flow: pressure, geometry of the combustion chamber, formulation.[4,17] However, the results obtained in quiescent atmospheres must be complemented by investigations under cross-flow conditions.

In these respect, Caveny and Gany[10] conducted a pioneeristic study, investigating aluminum agglomerates in an accelerating environment. Photographing the flame zone above thin strips of aluminized propellant, cast between sections of non-aluminized one, they were able to visualize individual agglomerates. High-speed, high-magnification camera allowed slow motion viewing of combustion phenomena with minimum interference. However, their results in terms of agglomeration, sensitivity to pressure and to mass fraction of aluminum are limited to a Mach number up to 0.2. The purpose of the experimental section of this work is to further extend the knowledge on the agglomerates behaviour, by recording their evolution in a gas-dynamic nozzle.

2.2 2D Windowed Rocket Motor Experimental Setup
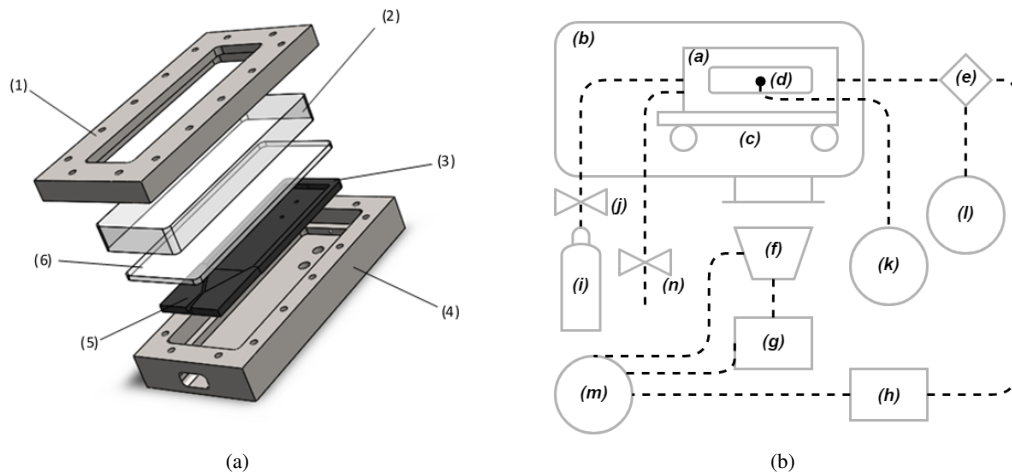
Figure 1: Experimental setup. Left - 2D Windowed rocket motor sketch: (a) top closing; (b) pressure-resistant window; (c) combustion chamber mold; (d) housing; (e) nozzle; (f) heat-resistant window. Right - sketch of the experimental facility

Experiments were conducted using a two-dimensional windowed rocket motor, schematically shown in Fig. 1(a). The 20 cm motor uses parallel slabs of propellant up to 12 cm long and 5 mm thick, housed in the combustion chamber (3). The propellant is directly poured into the chamber for curing by means of appropriate molds. The throat area 2 x 5 mm grants to achieve the nominal conditions of 15 bar in the combustion chamber, then the flow is further expanded to ambient pressure (5). Two windows placed above the combustion chamber and the nozzle enable the visualization: the first one (2) has structural purposes, keeping the desired pressure level inside the combustion chamber; the second one (5) is a ceramic heat-resistant transparent glass. Ceramics has been chosen since it gets slightly opaque once directly

in contact with the flame, it does not deform and its transparency can be easily restored. However, being a fragile material, particular attention must be given to the sealings of the system. The experimental line, sketched in Fig. 1(b) consists of:

- protection system to ensure safety during operations: a vessel housing the entire system (b) and safety relief valves in case of overpressure (i.e., throat blockage) (n);

- rocket motor (a) and support system (c), avoiding motion of the former during operations;

- pressure transducer (e) to record pressure during functioning and its protection system, consisting of a non-return valve and protective nitrogen (i, j);

- squib starter ignition system (d);

- acquisition system (c-m);

- visualization equipment: high speed camera (f).

The accurate description of the flow field through photo sequence is the goal of the high speed camera, a device able to capture high quality images of the flow at high frame rate. A fast shutter time is required due to the high velocity at stake in order to "freeze" a fast object without blur, and at the same time a high frame rate is needed for a good tracking in space. Focal multipliers, extensions and telephoto lens are needed to reach a high magnification, since for the safety reason of dealing with a new apparatus the high speed video camera could not be put in proximity of the window. These devices reduce the amount of light reaching the camera image sensor, affecting in turn the depth of field which has to be reduced to increase the incoming light. This problem can be overcome considering the number of emitting Al/Al2O3 agglomerates (refer to Fig. 2(a)) which generates a very bright field. Unfortunately, the resulting bright clouds could hinder the examination of individual particles.
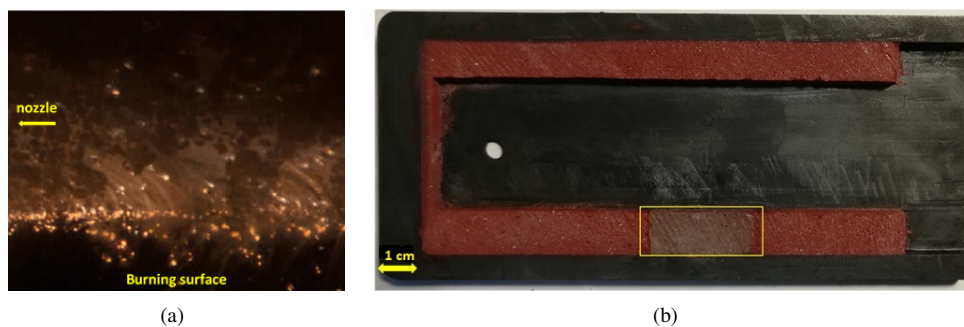
Figure 2: Experimental setup: (a) magnification of the burning surface of the aluminized propellant strip; (b) Aluminum-loaded propellant (yellow rectangle) inserted in the non-metallized slab.

As shown in Fig. 2(b), a single strip of Aluminum-propellant is inserted in the non-metallized propellants slabs to avoid excessive brightness and numbers of particles, as suggested by Caveny et al.[9] Neither the strips nor the propellant are cast in the mold, but directly poured for couring in the combustion chamber in two subsequent step.

2.3 Image Post-processing and Analysis

The images of the burning droplets were analysed by applying an in-house written Matlab routine, which incorporated several functions of the Matlab Image Processing Toolbox. The purpose of the code is (a) measure radial intensity slices through droplets and surrounding flames, (b) de-convolute these intensity profiles using an Abel inversion to obtain a true radial intensity profile. The code was developed following the work of Melcher et al.[20],[19] allowing semi-automatic measure of agglomerates diameter. As far as the speed is concerned, the distance between the positions of the centroid of the agglomerate between two consecutive frames is divided by the reciprocal of the frame rate, thus obtaining indications on an average speed.[25]

3. Numerical Activity

3.1 Solid rocket modelling: state of the art

Several efforts on numerical modelling of reacting and non-reacting particulate flows in SRMs were made in the past. Hwang et al.[15] developed an Eulerian-Lagrangian two-way coupled CFD analysis for several particle diameters, particle mixtures and mass loading, highlighting the influence on Mach number and temperature distribution of particles depending on their size.

Shimada et al.[30] studied the flow inside SRMs in relation to (a) nozzle throat ablation due to convective heat flux of the main flow and (b) abrasion due to aluminum/alumina particles. An eulerian approach was used for the gaseous field and the smoke oxide particles, while the lagrangian particles tacking was employed for the disperse phase.

Madabhushi et al.[16] calculated the two-phase flow field of the aft-dome region of the submerged nozzle of the Space Shuttle SRM. The analysis was carried out by coupling a lagrangian trajectory approach with an ensemble-averaged Navier-Stokes solution. The main focus of this study was on alumina slag accumulation in the side chambers of the nozzle geometry and the sensitivity of particle dynamics to the injection velocity, which was discovered being unrelevant.

Sabnis[28] modeled the combustion behaviour of a BATES type motor. A distributed combustion model was employed by applying an empirical combustion rate model to lagrangian particles in an equilibrium base flow. The distributed combustion results showed generally higher temperatures, gradually increasing towards the centerline. For particle breakup, Sabnis used a simplistic model based on a critical Weber number, describing the imbalance between drag force and surface tension on the droplet.

Ecker et al.[8] performed numerical investigations with the hybrid structured/unstructured DLR-Navier Stokes solver TAU, coupling steady state flow solutions and a lagranian particle trajectory methodology. Numerical studies on distributed aluminum combustion in the SRM combustion chamber were performed by combining models for evaporation and condensation as well as reaction mechanisms for nano-Al combustion. For some cases particle breakup was considered based on a critical Weber number. The contributions of condensation and evaporation were stated to be important in the reacting flow, mainly influencing temperature and species distribution within the chamber. On the contrary, the accurate predictions of the droplet diameters at the domain exit and plume regions is mainly influenced by droplet breakup.

3.2 Break-up modeling: state of the art

Liquid breakup regimes are typically divided into primary and secondary breakup. The former describes the breakup of the intact liquid phase into first ligaments and droplets. The latter describes how the relatively large initial droplets can be further distorted and subsequently broken up into smaller particles. It is primarily driven by aerodynamic forces employed on the drops by the surrounding gas phase. These forces cause a distortion of the initially spherical droplet that will eventually lead to breakup. When dealing with SRMs, the focus is on the secondary break up regime. As the gas surrounding velocity increases, the breakup level becomes more intense, in turn affecting the motor efficiency of the nozzle. In fact, liquid breakup in the nozzle throat reduces the liquid alumina droplet size, resulting in easier discharge of droplets by the carrier gas rather than alumina adhesion to the nozzle walls.[33] Consequently, if agglomerate breakup results in sufficiently small droplets, the agglomerates can burn completely inside the nozzle, reducing the fraction of unburnt aluminum. It has been reported that there should be approximately 1% I_{sp} loss every 10% unburnt aluminum.[22]

Several efforts have been made to properly describe the secondary breakup phenomenon. Many authors[9, 10, 28] point at the Weber number as the fundamental parameter at stake. Hence, the description of the imbalance between drag force and surface tension on the droplet is commonly considered a close-to-reality approximation of the phenomenon. Caveny and Gany identified that agglomerate breakup in SRMs conditions usually occurs when a Weber number of approximately 28 is reached.[9]

Pilch and Erdman made an extensive study on acceleration-induced droplet breakup processes.[26] Depending on the Weber number, five different breakup mechanisms have been identified (refer to Fig. 3). A critical We number, sufficient to complete the bag-type breakup, was defined by the introduction of the Ohnesorge (Oh) number, which reflects the relative importance between viscous forces and surface tension forces:

$$We_c = 12(1 + 1.077Oh^{1.6}) \tag{1}$$

Apart from the Weber-based models, the American Air's Force laboratories and the Aerojet Company[3] have identified a promising alternative in the Taylor Analogy Breakup (TAB) model. The TAB model, firstly introduced by O'Rourke et al.,[24] is based on the analogy between an oscillating and distorting droplet and a spring-mass system. The
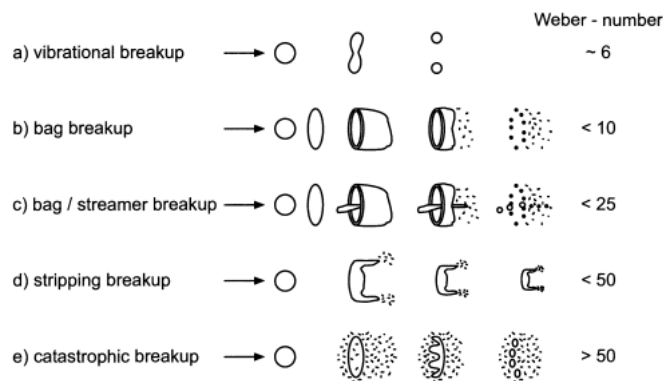
Figure 3: Droplet Breakup Regimes.[26]

restoring force of the spring is assumed to be analogous to the surface tension forces, the external force on the mass to the aerodynamic forces and the damping forces to the liquid viscosity effects, significantly affecting the oscillation of small drops. Droplet size evolution, bag breakup and stripping breakup events, velocity of the daughter droplets are well predicted by tracking one oscillation mode. However, it must be underlined that for large Weber numbers other modes than the lowest order spherical zonal harmonic (whose axis is aligned with the relative velocity vector between droplets and flow) are excited, contributing to drops breakup and hence limiting the applicability of the methods.

An improvement of the TAB model is the ETAB (i.e., Enhanced Taylor Analogy Breakup Model).[31,32] It was developed in the automotive framework to obtain realistic information about penetration, radial expansion and cross-sectional drop size distributions of sprays. A cascade of droplets breakups is considered and the rate of child droplet generation is modeled as proportional to the number of child droplets. Moreover, the percentage of drop deformation velocity that goes into the normal velocity component of the products droplets is added to the model.

The present work aims at presenting the results of the application of the model by Pilch and Erdman[26] and the ETAB[31,32] to the alumina particles evolution in the nozzle.

3.3 OpenFOAM Solver description

3.3.1 Eulerian Gas phase

All numerical investigations in the present study were performed within the OpenFOAM - Open Source Field Operation and Manipulation - framework, a widely known open source toolbox for Computational Fluid Dynamics. The *rhoCentralFoam*[12] density-based compressible flow solver based on central-upwind schemes of Kurganov and Tadmor has been employed for solving the Navier-Stokes equations coupled with the k-ω SST turbulence model. In particular, solution of momentum and energy transport is performed by a predictor equation for the convection of conserved variables followed by a corrector equation for diffusion of primitive variables. This enables the convection component to be solved quickly with a diagonal solver, while the diffusion component is solved implicitly to assist stability.

3.3.2 Lagrangian Particle Tracking

The Lagrangian Particle Tracking library, introduced by Nordin[23] has been coupled with the original baseline of *rhoCentralFoam*. In this approach parcels (i.e., computational group of particles with same properties) or clouds (i.e., container of objects of type parcels, thus describing the polydispersity of the disperse phase) are used to account for solid/liquid phase in a Lagrangian framework. The motion of each parcel or cloud is governed by Newton's second law and it is described by solving a set of ordinary differential equations along the trajectory. The influence of the dispersed phase on the main flow is assessed by considering the source terms for mass, momentum and energy, which are introduced in the algorithm in the predictor step before the diffusion correction. Depending on the nature of the problem, and thus on the variable of interest, the source terms are modeled according to different LTP libraries (refer to Fig. 4). The *basicSprayCloud* library, typically considered for sprays in the automotive field, is selected for the present work. It considers a cloud of spray reacting parcels, adding functionalities for atomization and breakup to the particles kinematic and thermal description.

Library	Major Variables	Variables being updated
solidParticle	vel., pos., d	vel., pos.
KinematicParcel	vel., pos., d	vel., pos.
CollidingParcel	vel., pos., d	vel., pos.
ThermalParcel	vel., pos., d , and T	Everything but d
ReactingParcel	vel., pos., d , T, and Y	Everything but d
ReactingMultiphase	vel., pos., d , T, Y, YLiquid , YSolid	Everything

Figure 4: Main LPT libraries in OpenFOAM.

3.3.3 Al2O3 Properties

A file defining the thermophysical behaviour of the aluminum oxide must be included in an ad-hoc OpenFOAM library which describes liquid substances to be treated as drops. The required properties are listed in Table 1.

Table 1: Thermophysical properties required by the OpenFOAM library.

Molecular weight [kg/kmol]	Critical temperature [K]
Critical pressure [Pa]	Critical volume [m^3/kmol]
Critical pressure [Pa]	Critical volume [m^3/kmol]
Critical compressibility factor []	Triple point temperature [K]
Triple point pressure [Pa]	Normal boiling temperature [K]
Dipole moment []	Pitzer's acentric factor []
Solubility parameter [$(J/m^3)^{0.5}$]	density [kg/m^3] as a function of temperature
Vapour pressure [Pa] as a function of T	Heat Capacity [J/kg] as a function of T
Liquid enthalpy [J/kg] as a function of T	Vapour heat capacity [J/(kg K)] as a function of T
Liquid viscosity [Pa s] as a function of T	Vapour viscosity [Pa s] as a function of T
Liquid thermal conductivity [W/(m K)] as a function of T	Vapour thermal conductivity [W/(m K)] as a function of T
Surface tension [N/m] as a function of T	Vapour diffusivity [m2/s] as a function of T

Since alumina is a refractory substance, vapour dynamic viscosity, vapour thermal conductivity, heat of vaporization and ideal gas heat capacity have no physical meaning and are not considered. The fitting functions depending on the temperature belong to the *NSRDSfunction* family. As example, the *NSRDfunc5*[5] is usually used to fit the density:

$$x = \frac{A}{B^{\left(1+\left(1-\frac{T}{C}\right)^D\right)}} \tag{2}$$

From the trend portrayed in Fig. 5, it is possible to compute the coefficients needed for the fitting: A = 1.03521527e+04, B = 1.53830661e+00, C = -9.55334805e+06, D = 2.91795155e+03. Refer to Daubert et al.[5] for further information.

3.4 Numerical Setup

The geometry of the 2D rocket motor is shown in Fig. 6. The throat is located at $x = 0.042m$, the exit at $x = 0.064m$ and the entrance section of the nozzle at $x = 0m$. It is possible to identify three different inlet patches, resembling the experimental configuration of Fig. 2(b): two inlets for the non-metallized propellant, one for the Al-loaded propellant. All walls are considered viscous walls and adiabatic. Temperature and pressure are specified at each inlets, while the velocity is derived accordingly. Ambient pressure is specified at the outlet by means of the *wavetransmissive* boundary condition which aims at minimizing numerical spurious reflections. A symmetry plane is defined on the x axis. The Software CEA is used to compute the mass fractions of the combustion products as well as the combustion chamber temperature, imposing the target pressure and the known expansion ratio. An artificial species is defined as a weighted average of all the species resulting from CEA computation for the selected inlet.
The specific heat, the enthalpy and the entropy curves of each CEA products as a function of temperature as well as the molecular mass, the enthalpy of formation and the molar fraction are used to define the resulting mixture thermophys-
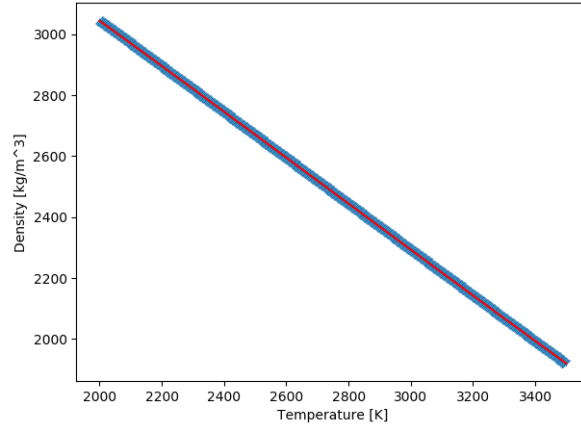
Figure 5: Density vs temperature.[27]
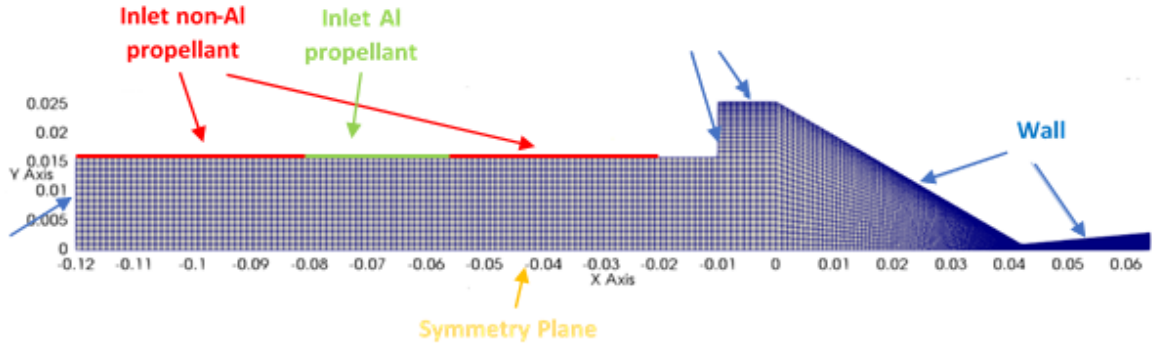
Figure 6: 2D Windowed rocket Motor geometry sketch.

.

ical properties. In particular, the weighted average quantities can be computed via the following formula:

$$f(T)_{averaged} = \sum_{i=1}^{N} \frac{f(T)_i Y_i}{Y_{tot}} \tag{3}$$

where $Y_{tot} = 1$ by definition.

The thermodynamic data for the individual species are conveniently stored in the form of coefficients of specific equations that fitting the data[2][11].[14] The equations used for the specific heat, enthalpy and entropy are:

$$\frac{C_p(T)}{R} = \sum_{i=1}^{r} a_i T^{(i-1)} = a_1 + a_2 T + a_3 T^2 + a_4 T^3 + a_5 T^4 \tag{4}$$

$$\frac{H(T)}{RT} = \frac{b_1}{T} + \frac{\int C_p(T)dT}{RT} = a_1 + a_2 \frac{T}{2} + a_3 \frac{T^2}{3} + a_4 \frac{T^3}{4} + a_5 \frac{T^4}{5} + \frac{b_1}{T} \tag{5}$$

$$\frac{S(T)}{R} = b_2 + \int \left(\frac{C_p(T)}{RT} \right) dt = a_1 \ln T + a_2 T + a_3 \frac{T^2}{2}$$
$$+ a_4 \frac{t^3}{3} + a_5 \frac{t^4}{4} + b_2 \tag{6}$$

where for $r = 5$ and a_i are the coefficients obtained from the fitting, b_1 and b_2 are integration constants. After defining the average curves for a specific temperature range, the coefficients for the fourth order equations of the JANAF model were obtained by fitting the data relative to the average curves of each mixture species. Sutherland model is used for

PARTICULATE PHASE EVOLUTION INSIDE SOLID ROCKET MOTORS: PRELIMINARY RESULTS

the computation of the viscosity.

The main assumptions considered in this work are then summarized:

- no chemical reactions nor combustion;

- each particle is considered composed only by liquid Al2O3. In reality, each particle is composed by aluminum covered by a layer of Al2O3. While in the combustion chamber, the particle could break and the Al inside could escape from the Al2O3 shell. This phenomenon is extremely complex from the chemical and physical point of view. A deeper analysis beyond the scope of this work is required to properly describe this phenomenon.

- no phase change of the liquid particles (in the temperature range considered the Al2O3 should remain liquid) and hence no mass exchange between phases.

4. Results

4.1 Break up models comparison
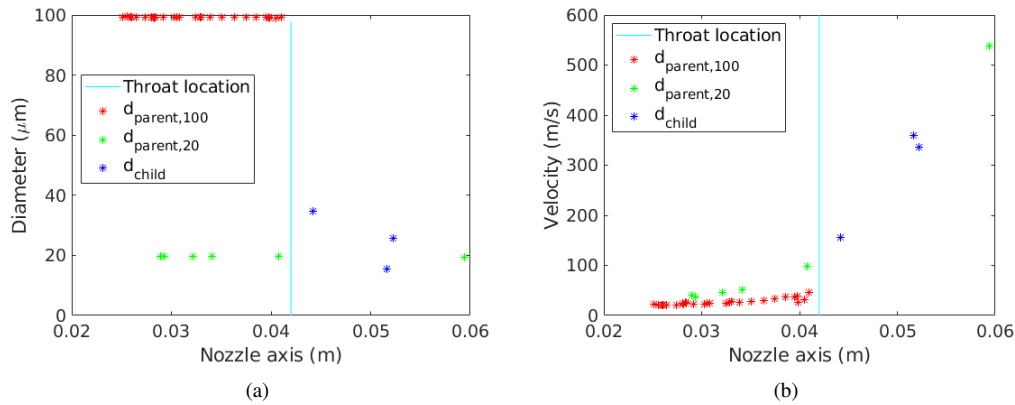
Figure 7: ETAB Model: (a) droplets diameter distribution. (b) droplets velocity distribution.
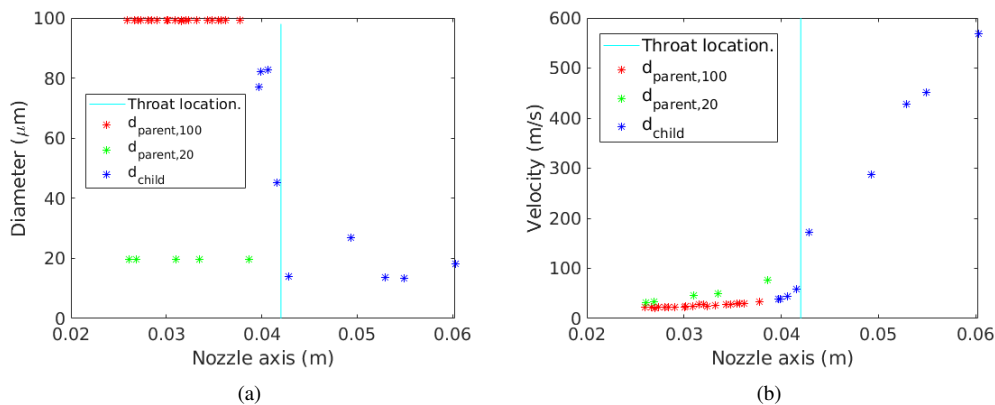
Figure 8: Pilch-Erdman Model: (a) droplets diameter distribution. (b) droplets velocity distribution.

The ETAB and Pilch-Erdman breakup models are investigated in the present section, paying attention mostly to the location where the breakup occurs and to the distribution of the droplet sizes affected by the breakup. A combustion chamber pressure of 15 bar is set, and a mass fraction of 5% of Aluminum is considered for the metallized propellant. The temperature of the three inlet patches is fixed according to CEA results: 2934 K for aluminized surface, 2731 K for the non-aluminized ones. Two modes of the experimentally obtained PSD are considered: 1/3 of the particles is assumed to have dimension of 20 μm and the remaining 2/3 of 100 μm.

Results in terms of diameters and velocities at different position along the nozzle towards the exit are displayed in Figs. 7 and 8. The identifier $d_{parent,100}$ defines the parent cloud with a diameter equal to 100 μm (red dots), $d_{parent,20}$ specifies the parent cloud with a diameter equal to 20 μm (green dots) and d_{child} considers the droplets after breakup (blue dots). Both the models well predict the occurrence of the breakup in the vicinity of the throat, displayed by a light blue line, caused by the huge velocity gradients of the main flow in turn affecting the relative velocity between the latter and the particles. The Pilch Erdman model considers a critical Weber number of 12 for breakup to occurr, while the ETAB model defines the its occurrence depending on a distortion parameter that includes the flow-particle dynamic interaction, surface tension and viscosity, thus not requiring an unique We number. Those differences are responsible of the slightly anticipated starting point of break up of Pilch-Erdman with respect to ETAB. Qualitatively speaking, particles with diameter higher than 40 μm are not present after the throat (i.e., x = 0.41 m) and a particle will keep breaking up till reaching a stable diameter, which in this condition appears to be around 20 μm for both the methods. It is interesting to note that considering a critical fixed Weber number of 12 would lead to multiple break up before reaching a "stable" configuration, while intermediate child droplets are not computed by the ETAB model. The two methods equally describe the trend of the velocity, highlighting the strong acceleration once in a divergent part up to 550 m/s (against a flow velocity of 1400 m/s).

4.2 Qualitative Experimental Results

Preliminary tests to assess the possibilities and limitations of the experimental apparatus have been performed and the main qualitative outcomes are hereby presented.

Table 2: Fast camera settings for the experimental tests.

Formulation	Setting (resolution - aperture - exposure time - frame rate)	Objective
Al 5%	21 pixel/mm - f/11 - 60μs - 3000fps	Overall agglomerate trajectory, camera settings
Al 5%	7 pixel/mm - f/8 - 60μs - 3000fps	d, V measurement
Al 18%	42 pixel/mm - f/8 - 40μs - 6000fps	Overall agglomerate trajectory, camera settings

The test matrix in Table 2 underlines three main activities required to tune the visualization apparatus and the camera settings: the overall flowfield visualization and agglomerates tracking for both 5% Al and 18% Al and the measurement of the diameter and velocity for the 5%Al-loaded propellant strip.

The amount of burning agglomerates and their detachment has been shown in Fig. 2(a). Their trajectory is reconstructed by means of a frame-by-frame manual analysis. The agglomerate protrudes initially vertically from the burning surface and it is then subjected to an horizontal cross flow which eases its detachment. The detaching angles of the particles ranges between 60° and 25°, decreasing moving towards the nozzle because of the well established gaseous cross flow. A burning surface magnification of the non-metallized propellant (refer to Fig. 9(a)) clearly highlights thee diffusive flame described by the Beckstead, Derr and Price Model (BDP).
Close-up footage in proximity of the nozzle throat confirmed this area as the mostly prone to break up events (see Fig. 9(b)). The two diverging tails leaving a bright discrete point can be tracked to identify the two fractions of the broken agglomerate. The bright lines in the core flow identify the agglomerates evolving through the nozzle.

(a)   (b)
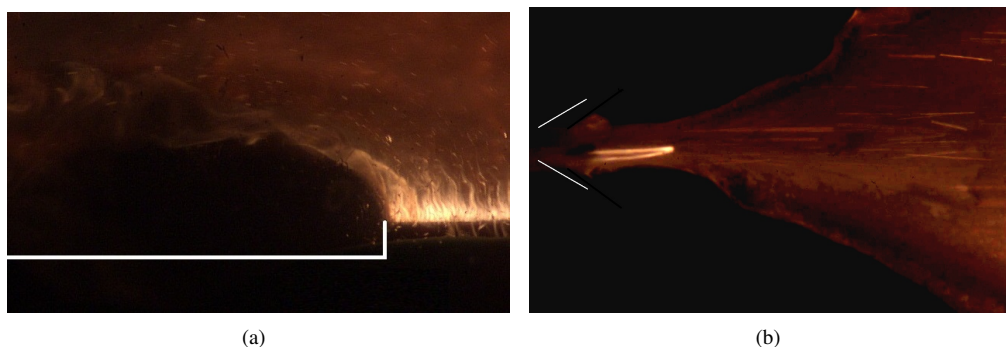
Figure 9: Experimental visualization at P = 5.6 bar (a) diffusive flame for a non-metallized propellant; (b) break-up events;

PARTICULATE PHASE EVOLUTION INSIDE SOLID ROCKET MOTORS: PRELIMINARY RESULTS

4.3 Experimental vs Numerical Results

A comparison between experimental and numerical data is investigated in the present section. A combustion chamber pressure of 5.6 bar is set, and a mass fraction of 5% of Aluminum is considered for the metallized propellant. The temperature of the three inlet patches is fixed according to CEA results: 2876 K for the aluminized surface, 2731 K for the non-aluminized ones. Two modes of the experimentally obtained PSD are considered: 1/3 of the particles is assumed to have dimension of 20 μm and the remaining 2/3 of 122 μm.
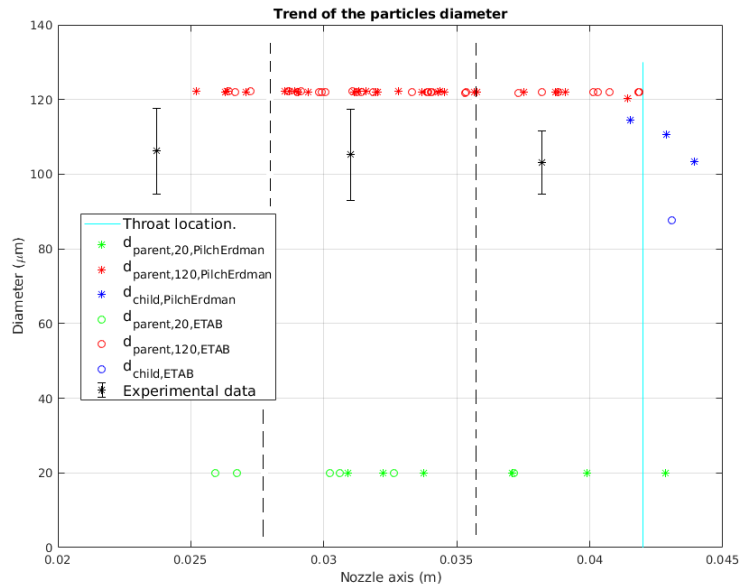
(a)
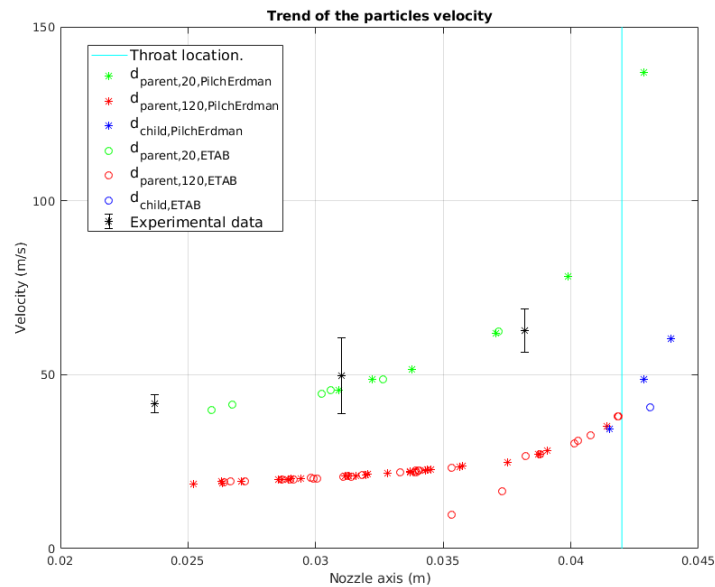
(b)

Figure 10: Qualitative Comparison: (a) droplets diameter distribution. (b) droplets velocity distribution. Parent clouds and child distribution are magnified by using different colors.

Three values of the agglomerates diameter with bars error from averaging of the experimental outcomes within the three black-dotted sections, comprising the convergent and the throat area, are superimposed to the numerical

results. Parent and child distributions are depicted with different colors. The experiments and numerical simulations differ in terms of the initial condition of the agglomerate diameters (i.e., 100 *mum* with respect to 120 *mum*). Despite this slight shift, an overall agreement in the trend of the variables can be appreciated in Figs. 10. The pressure level of 5.6 bar hinders the break up mechanism, fixing the "stable" diameter of the particles at 100 μm, matching the measured value in the throat-dotted section. The overall relative maximum errors is 18%. The visualizations confirm the major occurrence of breakup in the throat region, in accordance to the numerical outcomes. It has to be considered that different phenomena such as mass exchange between particles and flow, chemical reactions and combustion which are neglected in the numerical works, may partially influence the diameter evolution. However, those effects can be considered important inside the combustion chamber and in the initial part of the convergent. Afterwards, break up is the main driving mechanism of the PSD evolution. Due to the difference in terms of initial diameter, different velocities between numerical and experimental works arise. However, the trend is well matched. It is worth noting that the difference may be partially due to the higher density of the simulated particles with respect to the real ones (since the presence of aluminum is neglected in the numerical computation) as well as to an overestimation related to measurement of bright blurry object. Hence, the present comparison is for pure qualitative purpose since an experimental campaign focused on the improvement of the database of results is required for a quantitative discussion.

5. Conclusion

The present study aims at giving an overview of two novel techniques for particle size measurement in solid rocket motors. A 2D windowed rocket motor has been designed and the burning of aluminized propellant strips recorded. High speed video camera enabled to record the agglomerates evolution inside a gas dynamic nozzle at a pressure level of 5.6 bar and to obtain preliminary results suggesting the quality of the experimental concept. The results in terms of diameters and velocities have been superimposed to numerical simulations outcomes performed in the OpenFOAM environment. An eulerian gas phase description has been coupled to a Lagrangian particle tracking by means of already existing and to-be-implemented libraries. Two break models have been investigated: the Weber number-based break up model of Pilch-Erdman and the ETAB model based on the analogy between an oscillating and distorting droplet and a spring-mass system. The trend and absolute value of diameters and velocities are well matched by the two model, both indicating the throat region as the most important section for break up events. Experimental visualization confirmed this qualitative results, recording break up concentrated around the throat regions. A relative error of 18% between numerical and experimental results and the agreement on the final agglomerate at the throat sections, demand for an increase in the experimental available database and visualization equipment.

References

[1] A. G. Butler. Holographic investigation of solid propellant combustion. *Post-Graduate thesis. Naval Postgraduate School*, 1988.

[2] M. W. Chase. Janaf thermochemical data. *Journal of Physical and Chemical Reference Data*, 30:475–513.

[3] Hylin E. C. Babbitt D. Tullos J. A. Beckstead M. Webb M. Davis I. L. Dang A. Coats, D. Aluminum agglomeration and trajectory in solid rocket motors. *Final technical report. Software and Engineering Associates, Inc.*, 2007.

[4] C. T. Crowe and P. G. Willoughby. A study of particle growth in a rocket nozzle. *AIAA Journal*, 5(7):1300–1304, 1967.

[5] T. E. Daubert and R. P. Danner. *Data Compilation Tables of Properties of Pure Compounds Design Institute for Physical Property Data*. Design Institute for Physical Property Data, American Institute of Chemical Engineers, 1985.

[6] L. T. De Luca. *Problemi Energetici in Propulsione Aerospaziale (in Italian)*. Premani, 1999.

[7] Le Besnerais C. Nugue M. Devillers, R. W. and N. Cesco. Experimental analysis of solid-propellant surface during combustion with shadowgraphy images: new tools to assist aluminum-agglomeration modelling. *7th European Conference for Aeronautics and Aerospace Sciences (EUCASS)*, 2017.

[8] T. Ecker, S. Karl, and K. Hannemann. Modeling of aluminum particle combustion in solid rocket combustion chambers. In *AIAA Paper N. 2017-4781*.

PARTICULATE PHASE EVOLUTION INSIDE SOLID ROCKET MOTORS: PRELIMINARY RESULTS

[9] A. Gany and L. H. Caveny. Breakup of Al/Al2O3 agglomerates in accelerating flowfields. *AIAA Journal*, 17(12):1368–1371, 1979.

[10] A. Gany, L. H. Caveny, and M. Summerfield. Aluminized solid propellants burning in a rocket motor flow field. *AIAA Journal*, 16(7):736–739, 7.

[11] S. Gordon, B. J. McBride, and F. J. Zeleznik. *Computer Program Calculation of Complex Chemical Equilibrium Compositions and Applications, Supplement 1 - Transport Properties*. NASA Technical Memorandum, NASA - national Aeronautics and Space Administration, 1984.

[12] C. J. Greenshields, H. G. Weller, L. Gasparini, and J. M. Reese. Implementation of semi-discrete, non-staggered central schemes in a colocated, polyhedral, finite volume framework, for high-speed viscous flows. *International Journal for Numerical Methods in Fluids*, 63(1):1–21, 2010.

[13] V. G. Grigor'ev, V. E. Zarko, and K. P. Kutsenogii. Experimental investigation of the agglomeration of aluminum particles in burning condensed systems. *Combustion, Explosion and Shock Waves*, 17(3):245–251, 1981.

[14] L. V. Gurvich, I. V. Veits, and C. B. Alcock. *Calculation of thermodynamic properties.* Hemisphere, 1989.

[15] C. J. Hwang and G. C. Chang. Numerical study of gas-particle flow in a solid rocket nozzle. *AIAA Journal*, 26(6):682–689, 1988.

[16] R. K. Madabhushi, J. S. Sabnis, F. J. De Jong, and H. J. Gibeling. Calculation of the two-phase aft-dome flowfield in solid rocket motors. *Journal of Propulsion and Power*, 7(2):178–184, 1991.

[17] F. Maggi, S. Dossi, and L. T. DeLuca. Combustion of metal agglomerates in a solid rocket core flow. *Acta Astronautica*, 92(2):163–171, 2013.

[18] F. E. Marble. Droplet agglomeration in rocket nozzles caused by particle slip and collision. *Acta Astronautica*, 13(2):159–166, 1967.

[19] J. Melcher, R. Burton, and H. Krier. Combustion of aluminum in solid rocket motor flows. *AIAA paper No. 2000-3333*.

[20] J. Melcher, R. Burton, and H. Krier. Burning aluminum particles inside a laboratory-scale solid rocket motor. *Journal of Propulsion and Power*, 18(3):631–640, 2002.

[21] Son F. Sivathanu Y.R. Moore, J.E. and J. Lim. Experimental characteristics of particle dynamics within solid rocket motors environments. Technical paper & briefing charts, Air Force Research Laboratory (AFMC), 2009.

[22] W. Netzer et al. Particle behavior in solid propellant rockets. *NASA. The 17th JANNAF Combustion Meeting, Langley Research Center*, 1(SEE N81-16253 07-28):1–20, 1980.

[23] P. A. N. Nordin. *Complex chemistry modeling of diesell spray combustion*. Chalmers University of Technology, Sweden, 2000.

[24] P. J. O'Rourke and A. A. Amsden. The tab method for numerical calculation of spray droplet breakup. Technical report, SAE Technical Paper, 1987.

[25] A. Paradiso. Algoritmo per la misura semiautomatica della dimensione degli agglomerati di un propellente solido alluminizzato (in italian). *M.Sc. Thesis, Politecnico di Milano*.

[26] M. Pilch and C. A. Erdman. Use of breakup time data and velocity history data to predict the maximum size of stable fragments for acceleration-induced breakup of a liquid drop. *International Journal of Multiphase Flow*, 13(6):741–757, 1987.

[27] J. J. Rasmussen. Surface tension, density, and volume change on melting of Al2O3 systems, Cr2O3, and Sm2O3. *Journal of The American Ceramic*, 55(6):326.

[28] J. S. Sabnis. Numerical simulation of distributed combustion in solid rocket motors with metalized propellant. *Journal of Propulsion and Power*, 19(1):48–55.

[29] M. Salita. Use of water and mercury droplets to simulate al2o3 collision/coalescence in rocket motors. *Journal of Propulsion and Power*, 7(4):505–512, 1991.

[30] T. Shimada, M. Sekiguchi, and N. Sekino. Flow inside a solid rocket motor with relation to nozzle inlet ablation. *AIAA Journal*, 45(6):1324–1332, 2007.

[31] F. X. Tanner. Liquid jet atomization and droplet breakup modeling of non-evaporating diesel fuel sprays. *SAE Technical Paper Series*, 106(3):127–140, 1997.

[32] F. X. Tanner and G. Weisser. Simulation of liquid jet atomization for fuel sprays by means of cascade drop breakup model. *SAE Technical Paper Series*, 1998.

[33] Y. Yen. Numerical and experimental study of liquid breakup process in solid rocket motor nozzle. *PhD thesis, University of Wisconsin-Milwaukee*, 2016.